Experimental Neurology 311 (2019) 125–134

Contents lists available at ScienceDirect

Experimental Neurology

journal homepage: www.elsevier.com/locate/yexnr

Research paper

Self-reinforcing effects of mTOR hyperactive neurons on dendritic growth

Salwa R. Arafa[a,b], Candi L. LaSarge[a], Raymund Y.K. Pun[a], Shadi Khademi[a], Steve C. Danzer[a,c,*]

[a] Department of Anesthesia, Cincinnati Children's Hospital Medical Center, Cincinnati, OH 45229, United States
[b] Department of Drug Development, James L Winkle College of Pharmacy, University of Cincinnati, OH 45267, United States
[c] Departments of Anesthesia and Pediatrics, University of Cincinnati, Cincinnati, OH 45267, United States

A B S T R A C T

Loss of the mTOR pathway negative regulator PTEN from hippocampal dentate granule cells leads to neuronal hypertrophy, increased dendritic branching and aberrant basal dendrite formation in animal models. Similar changes are evident in humans with mTOR pathway mutations. These genetic conditions are associated with autism, cognitive dysfunction and epilepsy. Interestingly, humans with mTOR pathway mutations often present with mosaic disruptions of gene function, producing lesions that range from focal cortical dysplasia to hemimegalanecephaly. Whether mTOR-mediated neuronal dysmorphogenesis is impacted by the number of affected cells, however, is not known. mTOR mutations can produce secondary comorbidities, including brain hypertrophy and seizures, which could exacerbate dysmorphogenesis among mutant cells. To determine whether the percentage or "load" of PTEN knockout granule cells impacts the morphological development of these same cells, we generated two groups of PTEN knockout mice. In the first, PTEN deletion rates were held constant, at about 5%, and knockout cell growth over time was assessed. Knockout cells exhibited significant dendritic growth between 7 and 18 weeks, demonstrating that aberrant dendritic growth continues even after the cells reach maturity. In the second group of mice, PTEN was deleted from 2 to 37% of granule cells to determine whether deletion rate was a factor in driving this continued growth. Multivariate analysis revealed that both age and knockout cell load contributed to knockout cell dendritic growth. Although the mechanism remains to be determined, these findings demonstrate that large numbers of mutant neurons can produce self-reinforcing effects on their own growth.

1. Introduction

Genetic lesions that impact the mechanistic target of rapamycin (mTOR) signaling pathway cause a range of human diseases. Examples include tuberous sclerosis complex (TSC1 and TSC2), focal cortical dysplasia (AKT3, TSC1, PTEN, PIK3CA, mTOR), hemimegalencephaly (AKT3, PIK3CA, mTOR) and Cowden syndrome (PTEN) (Crino, 2011; Wong and Crino, 2012; Krueger et al., 2013; Lasarge and Danzer, 2014; Marsan and Baulac, 2018). These aptly named "mTORopathies" can result from germline or somatic mutations. Intriguingly, somatic mutations can impact widely varying numbers of cells. In hemimegalancephaly, for example, an entire hemisphere may be affected, while mutations may be present in only a small region of cortex in focal cortical dysplasia. This variability raises the possibility that neurons with mTOR mutations may follow different pathological trajectories depending on the number of surrounding cells that also exhibit the mutation. Excess mTOR signaling profoundly disrupts the morphology and function of neurons exhibiting the mutation, and widespread mutations can alter the gross structure of the brain, increase inflammation, alter network behavior and produce secondary pathologies, such as seizures (Ogawa et al., 2007; Zeng et al., 2008; Pun et al., 2012; Parker et al., 2013; Matsushita et al., 2016; Barrows et al., 2017; Wesseling et al., 2017). mTOR-mediated disruption of neuronal growth may precede independently of these secondary effects, or secondary changes may produce feedback effects, whereby mTOR mutant cells become increasingly pathological over time and as a function of the "load" of surrounding mutant cells.

To assess the impact of altering the load of mTOR mutant cells on the pathological development of these same cells, we developed a conditional, inducible PTEN knockout mouse model of epilepsy in which PTEN can be deleted from variable numbers of postnatally-generated hippocampal granule cells (Pun et al., 2012; LaSarge et al., 2015, 2016; Santos et al., 2017). At the single cell level, PTEN loss induces somatic hypertrophy, increases dendrite length and complexity (Kwon et al., 2001, 2003; Zhou et al., 2009; Urbanska et al., 2012; Sperow et al., 2012) and leads to the de novo appearance of hilar basal dendrites on hippocampal granule cells (Kwon et al., 2006; Lasarge and Danzer, 2014). At the systems level, PTEN loss can lead to gross brain hypertrophy, inflammatory changes, behavioral abnormalities and epilepsy (Kwon et al., 2001, 2006; Amiri et al., 2012; Pun et al., 2012; Lugo et al., 2014; Nguyen and Anderson, 2018).

Animals lacking PTEN from variable numbers of granule cells were generated in two cohorts. In the first, PTEN deletion rates were held at around 5%, and knockout cell growth over time was assessed. Previous studies have demonstrated that PTEN deletion leads to the rapid appearance of abnormalities over weeks (Luikart et al., 2011; Williams

* Corresponding author at: 3333 Burnet Avenue, ML, 2001 Cincinnati, OH, United States.
E-mail address: steve.danzer@cchmc.org (S.C. Danzer).

https://doi.org/10.1016/j.expneurol.2018.09.019
Received 29 May 2018; Received in revised form 17 September 2018; Accepted 27 September 2018
Available online 28 September 2018
0014-4886/

et al., 2015), but whether changes become progressively worse over months or eventually plateau is not known. In the second cohort, knockout cell deletion rates ranged from 2 to 37%, and the impact of both age and knockout cell load were assessed. These experiments reveal whether and how the mosaic nature of mTORopathies might impact the development of individual morphological abnormalities.

2. Materials and methods

All animal procedures were conducted in accordance with NIH and CCHMC Institutional Animal Care and Use Committee (IACUC) guidelines. All mice were maintained on C57BL/6 background. The following mouse strains were used for the present study: *Gli1-CreER^{T2}* mice (RRID: IMSR_ JAX STRAIN#007913), PTEN$^{flox/flox}$ mice (RRID: IMSR_JAX STRAIN #006440), and *Gt(ROSA)26Sortm1(CAG-Brainbow2.1)Cle/J* "*Brainbow*" reporter mice (RRID:IMSR_JAX STRAIN#013731). *Gli1-CreER^{T2}* mice express tamoxifen-inducible cre-recombinase in neuronal progenitor cells (Ahn and Joyner, 2005). PTEN$^{flox/flox}$ mice possess LoxP flanked "floxed" PTEN exon 5. Brainbow mice stochastically express GFP, YFP, CFP or RFP upon cre-recombination (Cai et al., 2013).

2.1. Brainbow-expressing PTEN knockout mice

Study animals were generated by crossing *Gli1-CreER^{T2}* hemizygous; *PTEN$^{flox/wt}$*; Brainbow$^{+/+}$ triple transgenic mice to *PTEN$^{flox/wt}$*; *Brainbow$^{+/+}$* double transgenic mice. The cross was used to generate the following genotypes:

1) *Gli1-CreER^{T2}* hemizygous; *PTEN$^{wt/wt}$*; *Brainbow$^{+/+}$* (Control, $n = 9$ male mice).
2) *Gli1-CreER^{T2}* hemizygous; *PTEN$^{flox/flox}$*; *Brainbow$^{+/+}$* (PTEN knockout [KO], $n = 11$ male mice).

All mice were injected with tamoxifen (Sigma Aldrich, T5648; 250 mg/kg dissolved at 20 mg/ml in corn oil, S·C) on post-natal day (P) 21 to delete PTEN and express the brainbow fluorophores. Brainbow control and KO mice were randomly assigned to one of two groups for perfusion 4 (7-weeks-old) or 15 (18-weeks-old) weeks after tamoxifen injection. Final experimental groups were as follows: 7-week-old group, 4 control and 5 KO; 18-week-old group, 5 control and 6 KO.

Brainbow-expressing control and KO mice were anaesthetized with pentobarbital (100 mg/kg, intraperitoneal) and transcardially perfused through the ascending aorta with ice-cold 0.1 M phosphate buffered saline (PBS, pH 7.4) containing 1 U/ml heparin for 1 min at 6 ml/min, immediately followed by a solution of 2.5% paraformaldehyde (PFA) with 4% sucrose in PBS for 10 min at 25 °C. Brains were removed and bisected along the sagittal plane into left and right hemispheres. The left hemisphere of each brain was post-fixed for 24 h and cryoprotected in 10%, 20%, and 30% sucrose in PBS for 24, 24, and 48 h, respectively. Left hemispheres were snap-frozen in 2-methylbutane chilled to −23 °C with dry ice and stored at −80 °C until sectioning. Left hemispheres were sectioned sagittally at a thickness of 60 μm using a cryostat maintained at −20 °C. Sections were thawed in PBS, slide mounted, air dried and stored at −80 °C for immunohistochemical tests. Right hemispheres were used to collect images for neuronal reconstructions for morphological analyses. Right hemispheres were post-fixed overnight and incubated in 10% sucrose in PBS for a minimum of 24 h; tissue was then cut into 1 mm coronal sections using a tissue slicer (Campden/Lafayette Instruments, IN). Sections were incubated for optical clearing in Sca*l*eA2 for 3–4 weeks at 4 °C (Hama et al., 2015; Singh et al., 2015) and preserved in Sca*l*eA2 until imaging.

2.2. Neuronal reconstructions of cells labeled in brainbow-expressing PTEN KO mice

One millimeter thick Sca*l*eA2 cleared tissue sections were imaged using a Nikon A1Rsi inverted microscope equipped with a 40× Plan Apo water immersion objective (NA = 1.15, field size 317 × 317 μm). Yellow fluorescent protein (YFP) and red fluorescent protein (RFP) expressing cell clusters in brainbow positive mice (PTEN KO and control) were imaged. Consistent with prior studies, cyan fluorescent protein (CFP) expressing nuclei were rare in CNS, and green fluorescent protein (GFP) expressing cells were not evident (Singh et al., 2015). Three dimensional z-series confocal image stacks were collected through up to 500 μm of the tissue at 1 μm increments to capture cells in their entirety. Between one and eight cells per animal were traced; except for one KO mouse in the 18-week group. In this animal, no brainbow-expressing PTEN KO cells were found. Cells with proximal dendrites cut at the tissue surface, or with dendrites that could not be clearly visualized were excluded. In KO animals, cells were also excluded if their soma areas were within two standard deviations of the mean of soma areas for control cells. These cells likely reflect brainbow-expressing, PTEN-expressing cells in KO animals resulting from incomplete cre-mediated recombination of the floxed PTEN gene. This criteria has been previously validated to distinguish > 95% of KO cells from control cells (Santos et al., 2017). Cells meeting reconstruction criteria were randomly selected for analysis.

Confocal z-series image stacks were imported to Neurolucida for whole cell tracing. Reconstructions encoded soma area, apical and basal dendrite length, and dendritic branch points. Image stacks were also used to encode the location of the hilar-granule cell body layer border, the granule cell body layer-molecular layer border, and the location of the hippocampal fissure. The molecular layer was further subdivided into inner (IML), middle (MML), and outer (OML) regions, with the inner region being the first 17% of the molecular layer (West and Andersen, 1980; Deller et al., 1999; van Groen et al., 2003; Santos et al., 2011), and the middle and outer being an equal split of the remainder.

2.3. Histology and immunohistochemistry

For the brainbow control and KO mice, sections at the same medial-lateral coordinates (Lateral 1.56; (Paxinos and Franklin, 2004)) were co-immunostained for PTEN/NeuN in order to quantify the percentage of PTEN KO cells. The following antibodies were used: mouse anti-NeuN (Neuronal nuclei protein, 1:400, Millipore Cat# MAB377 RRID:AB_2298772) and rabbit anti-PTEN antibodies (Phosphatase and tensin homolog, 1:250, Cell Signaling Technology Cat# 9559 RRID:AB_390810). Secondary antibodies included goat anti-rabbit Alex Fluor 594 (Thermo Fisher Scientific Cat# A11012 RRID: AB_10562717) and goat anti-mouse Alexa Fluor 647 (Thermo Fisher Scientific Cat# A-21242 RRID: AB_2535811), all at 1:750 dilution. Sections were dehydrated in serial alcohol washes, xylene cleared for 15 min, and hard mounted with Krystalon mounting medium (EMD Millipore, Cat# 64969).

2.4. PTEN KO cell counts

PTEN/NeuN immunostained sections were imaged with a Leica SP5 inverted microscope (software RRID: SCR_013673) equipped with 63× oil objective (NA = 1.4, field size 248 × 248 μm). Confocal z-series image stacks were collected through 7 μm of tissue at a 1 μm step, excluding the top 1–2 μm of tissue to avoid sectioning artifacts. A tile scan was used to capture the entire dentate gyrus in brain hemi sections, and images were imported to Neurolucida software (Microbrightfield Inc., RRID: SCR_001775) to stitch tiles together for dentate gyrus reconstruction. Two 100 × 100 μm counting frames were placed over the midpoints of the upper and lower blades of the dentate gyrus, respectively. The total number of NeuN positive cells, and the number of NeuN positive, PTEN negative (PTEN KO) cells within these frames was

determined. Counts were conducted using a modified optical dissector approach, with the top and left sides of the box set as exclusion zones. Using this methodology, cell bodies cropped at the surface or left sides of the counting frame were excluded. Exclusion zones were not needed for the top/bottom of the counting frame, as the natural borders of the dentate at the molecular layer and hilus were contained within the frame. All counts were completed by a reviewer blinded to treatment conditions. The percentage of KO cells was determined using the following equation: [total number of NeuN positive, PTEN negative [KO] cells divided by the total number of NeuN positive cells] X 100.

2.5. Biocytin-labeling of PTEN KO granule cells

In addition to the use of triple-transgenic brainbow-expressing mice, biocytin-filled cells from male and female double-transgenic *Gli1-CreER^{T2}* hemizygous; PTEN$^{flox/flox}$ mice were also used to assess cell structure. Biocytin-filled cells were selected from a previously-generated database of morphologically reconstructed granule cells. Physiological and morphological data from a subset of these cells is presented as part of another study (Santos et al., 2017). For the present study, all cells in the database meeting study inclusion criteria (animal genotype, cell genotype, tamoxifen protocol) and with complete data sets (morphological parameters collected and %KO determined) were included.

Double-transgenic mice were injected with 250 mg/kg tamoxifen on either P21 (n = 13 male, 1 female) – identical to brainbow-expressing animals – or P14 (n = 22 male, 6 female). Injecting the tamoxifen at an earlier age increases the number of PTEN KO cells in the animals and is associated with the development of epilepsy (Pun et al., 2012). For morphological measures of biocytin-filled PTEN KO granule cells, a range of 1–3 cells/mouse was analyzed for a total of 57 cells.

Cells were labeled with biocytin in acute hippocampal slices, which were prepared as previously described (LaSarge et al. 2015). All cells were injected with 0.2% biocytin using a "blind" approach with a patch clamp electrode (Pinault, 1996). Patching was conducted using an Eclipse FN1 Nikon upright microscope equipped with 10× (NA = 0.25) and 40× (NA = 0.8) objectives. Brightfield optics were used to place the electrode tip just above the inner 1/3 of the dentate granule cell body layer, where the majority of PTEN KO cells are found. After this point, the microscope optics were no longer used and patching was conducted blindly by lowering the electrode into the cell body layer. The first cell for which a stable membrane seal was obtained was filled. After cell labeling, slices were put into fixative (2.5% paraformaldehyde, 4% sucrose in PBS) and left overnight. The next day, slices were rinsed in PBS for 15 min, exposed to 0.5% Igepal in PBS for one hour, followed by a 2 h incubation in 1:300 streptavidin-Alexa Fluor 488 conjugate (Molecular Probes Cat# S32354 also S32354 RRID:AB_2315383) at room temperature. Slices were cover-slipped with ProLong Gold Antifade mounting media (Molecular Probes, Life Technologies, Cat# P10144). Slices were left to cure overnight and then stored at 4 °C until imaging. The left half of the brain from these animals was immersion fixed overnight (2.5% paraformaldehyde, 4% sucrose in PBS), and this tissue was prepared for histological studies in the same manner as the brainbow tissue.

2.6. Neuronal reconstruction of biocytin-filled cells in double-transgenic PTEN KO mice

Cells were imaged using a Nikon A1Rsi inverted microscope equipped with a 40× Plan Apo water immersion objective (NA = 1.15, field size 317 × 317 μm). Three-dimensional confocal image stacks were captured through the z-depth of the tissue at 0.5 μm increments to reveal cells in their entirety. Multiple image stacks were required to fully capture neurons in the x-y dimensions, so overlapping image stacks were three-dimensionally montaged into a single image for reconstruction using Neurolucida software. Reconstructions were conducted as described for cells expressing brainbow fluorophores. Even though patch electrodes were targeted to the inner third of the granule cell body layer – where most KO cells were located – the blind patch approach still yielded both PTEN KO and PTEN-expressing cells. Cells were identified as PTEN KOs only after reconstruction, therefore, using the same criteria that was applied to brainbow-expressing cells (soma area exceeds two standard deviations of the control cell mean; Santos et al., 2017). For the present study, 49.8% of all cells filled met criteria for KO cells. Only data from KO cells is presented in the current study.

In order to obtain the percentage of PTEN KO cells in mice used for biocytin-fills, PTEN immunohistochemistry was performed (as described for brainbow mice), but sections were co-stained with NeuroTrace 640/660 Deep-Red Fluorescent Nissl stain (Thermo Fisher Scientific Cat# N21483:AB_2572212) at a dilution of 1:300 instead of NeuN labeling. An identical quantification approach to that described for brainbow mice was used. Both Nissl- and NeuN-based counting approaches were found to be equally effective (Santos et al., 2017).

2.7. Statistical analysis

All data collection and analyses were conducted by investigators blind to animal age and genotype. Cell counts and neuronal reconstructions were generated by a first investigator, and then reviewed by a second to achieve consensus. Statistical tests were performed using Sigma Plot software (version 14.0, Systat Software, Inc., San Jose, CA, RRID: SCR_003210). Group differences among brainbow mice were assessed by two-tailed Student's t-test for data that met assumptions of normality and equal variance or by Mann-Whitney rank sum test for data that violated either assumption. For these analyses, four comparisons were made: genotype within age and age within genotype. The threshold for significance was adjusted for multiple comparisons using Bonferroni corrections (0.05/4 = 0.0125). Specific tests used are noted in the results. Group differences among biocytin-filled cells were assessed using multiple linear regression with animal age and the percentage of KO cells as independent variables. Values from male and female mice were found to be statistically indistinguishable and were binned for analysis (Santos et al., 2017 and data not shown). P-values < .05 were accepted as significant. Values are presented as means ± SEM or medians [25th–75th percentiles] unless otherwise noted.

2.8. Figure preparation

Confocal z-series image stacks acquired on the Nikon platform were converted from 12 bit to 8 bit RGB.tiff files using NIS-Elements software (version 4.500.00, Nikon). Figures were prepared using Sigma Plot software and Adobe Photoshop CS5 (version 12.0, Adobe Photoshop). Images of granule cells in Figs. 4, 6 and 7 are neuronal reconstructions (Walter et al., 2007; Murphy et al., 2011).

3. Results

3.1. PTEN KO cell morphological abnormalities become more severe with age

Three-week-old triple transgenic *Gli1-CreER^{T2}* hemizygous; *PTEN$^{flox/flox}$*; *Brainbow$^{+/+}$* (brainbow-expressing, PTEN KO) and *Gli-CreER^{T2}* hemizygous; *PTEN$^{wt/wt}$*; *Brainbow$^{+/+}$* (brainbow-expressing, control) mice were treated with tamoxifen to induce PTEN deletion and brainbow fluorophore expression among hippocampal granule cell progenitors. Animals were sacrificed at 7 or 18 weeks-of-age (4 and 15 weeks post injection). PTEN deletion rates among granule cells was statistically similar between the two age groups (7 weeks, n = 5 KO mice, 5.7% [2.4–10.9]; 18 weeks, n = 5, 5.1% [4.2–6.1]; p = .841, Mann-Whitney rank sum test [RST]).

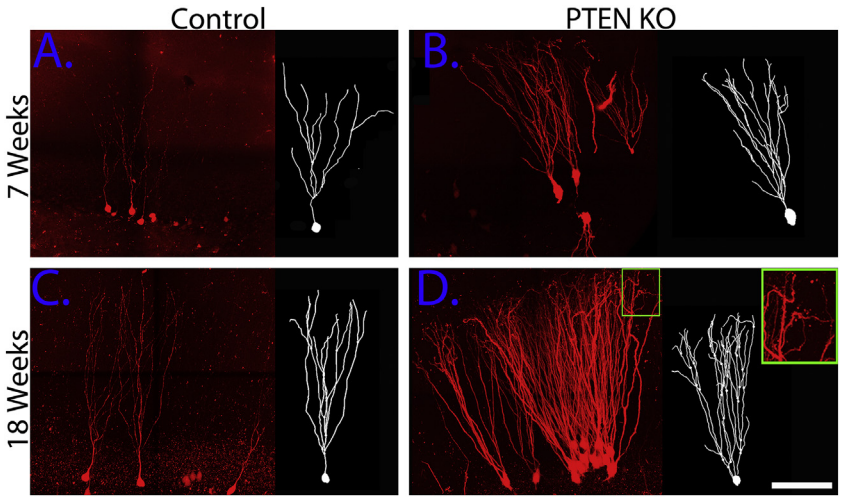

Fig. 1. Confocal maximum projections and representative Neurolucida reconstructions of brainbow-expressing cells in 7 and 18 weeks-old control (A, C) and KO (B, D) mice. The inset (green box) shows an expansion of outer molecular layer dendrites with processes growing parallel to the hippocampal fissure. Scale bar = 100 μm (200 μm for the inset). (For interpretation of the references to colour in this figure legend, the reader is referred to the web version of this article.)

3.2. Robust neuronal hypertrophy develops rapidly after cell birth

Somatic hypertrophy is the most consistent abnormality induced by PTEN deletion (Backman et al., 2001; Kwon et al., 2003, 2006; Pun et al., 2012). To examine the progression of somatic hypertrophy in control and KO animals, soma area measurements were collected from Sca*l*eA2 cleared tissue from 7- (control, $n = 15$ cells from 4 mice; KO, $n = 12$ cells from 5 mice), and 18- (control, $n = 23$ cells from 5 mice; KO, $n = 22$ cells from 5 mice) week-old mice. Fig. 1 shows clusters of brainbow-expressing KO and control cells at the different time points and a representative neuronal reconstruction from each cluster. PTEN KO cells showed dramatic somatic hypertrophy relative to control cells at both the 7 ($p \leq .0001$, *t*-test) and 18 week ($p < .001$, RST) time points (Fig.2A). These findings indicate that somatic hypertrophy increases rapidly (within a month) after PTEN deletion. To determine whether soma area increased between 7 and 18 weeks, we examined age changes within genotype. Among control animals, soma area did not change with age ($p = .817$, *t*-test). Although a trend towards increased soma area was observed within the KO groups, the difference did not reach the adjusted *p*-value for significance ($p = .0192$, *t*-test [threshold *p* value = .0125]).

3.3. PTEN loss increases apical dendrite length and complexity

Apical dendrite length has also been shown to increase following PTEN deletion (Jaworski et al., 2005; Kwon et al., 2006). To determine whether this increase progresses over the three months following PTEN deletion, YFP and RFP-expressing granule cells were examined in 7-

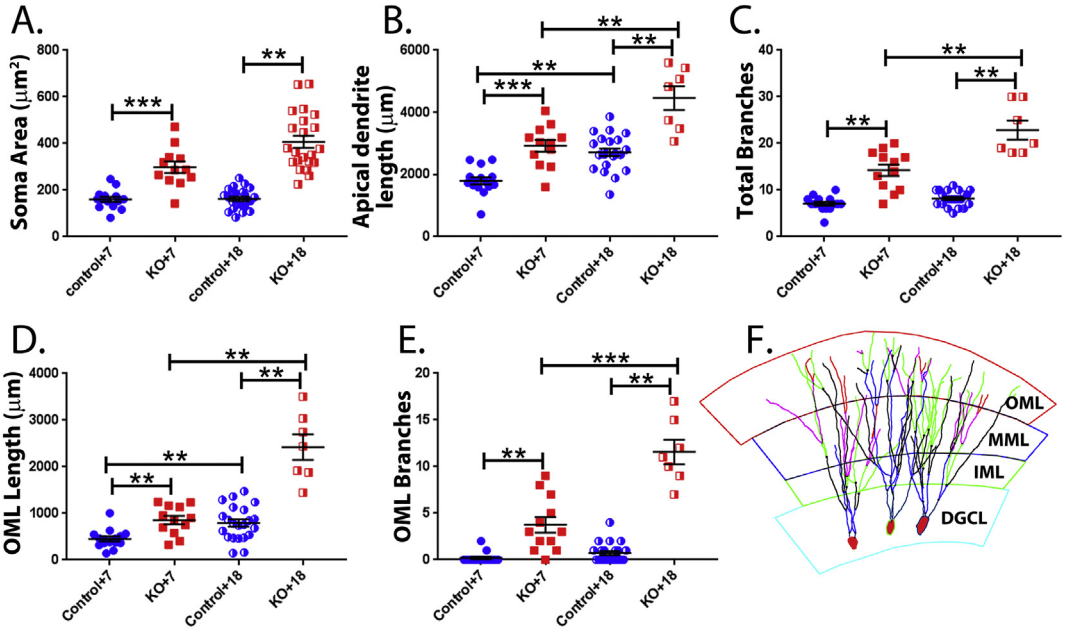

Fig. 2. Progression of morphological changes between 7 and 18 weeks for brainbow-expressing KO (red) and control (blue) cells. Each point in the graphs represents an individual granule cell, while bars depict means ± SEM. A: KO cell somas were larger than controls at both 7 and 18 weeks. B: Total apical dendrite length was greater for KO cells relative to controls at both 7 and 18 weeks, and both groups exhibited dendritic growth between 7 and 18 weeks. C: KO cell apical dendrites had more branches than controls at both 7 and 18 weeks. Between 7 and 18 weeks, dendritic branching increased among KO cells only. D: Dendrite length in the outer molecular layer was greater for KO cells relative to controls at both 7 and 18 weeks, and both groups exhibited dendritic growth between 7 and 18 weeks. E: KO cells had more branches than controls at both 7 and 18 weeks in the outer molecular layer. Between 7 and 18 weeks, dendritic branching increased among KO cells. F: The schematic shows the dentate granule cell layer (DGCL) and the three regions of the molecular layer (inner, IML; middle, MML and outer, OML) used for quantitative morphological analysis. *, $p < .0125$. **, $p < .0025$. ***, $p < .00025$ (Bonferroni-adjusted *p*-values). (For interpretation of the references to colour in this figure legend, the reader is referred to the web version of this article.)

week-old mice (control, $n = 15$ cells from 4 mice; KO, $n = 12$ cells from 5 mice) and 18-week-old mice (control, $n = 22$ cells from 5 mice; KO, $n = 7$ cells from 3 mice). Apical dendritic length was significantly greater for KOs in comparison to controls at both time points (Fig.2B; 7 weeks: $p \leq .0001$, *t*-test; 18 weeks: $p \leq .001$, RST). Analysis of age within controls revealed growth over time, with the apical dendritic trees in the 18 week group being larger than the 7 week group ($p \leq .001$, t-test). Dendritic lengthening among KO cells was also evident ($p \leq .001$, t-test). In addition to increased length, the total number of dendritic branch points per cell was significantly higher among KOs relative to controls at both 7 (Fig.2C; $p < .001$, RST) and 18 weeks ($p \leq .001$, RST). Among control cells, total branch number did not change significantly over time ($p = .046$, t-test [threshold p value = .0125]), while branch number increased significantly between 7 and 18 weeks among KOs ($p = .001$, t-test). These findings indicate that the apical dendrites of control cells show modest increases in dendrite length between 7 and 18 weeks, while KO cells show more robust increases in length and develop greater complexity over the same period.

3.4. Apical dendritic length by molecular layer subregion

Dentate granule cell apical dendrites project through three subregions within the dentate known as the inner, middle, and outer molecular layers. The inner molecular layer receives associational/commissural afferents, while the middle and outer molecular layers are innervated by medial and lateral entorhinal cortex, respectively (Deller et al., 1999; Dimoka et al., 2003; Förster et al., 2006; Amaral et al., 2007). To determine whether PTEN deletion has selective effects on specific dendritic compartments, we conducted subregion specific analyses (Fig. 2F).

Apical dendrite length contained within the inner molecular layer was significantly increased in brainbow-expressing 7 weeks-old KOs relative to their age-matched controls (Graphs not shown; controls: 305.5 ± 40.0 μm; KOs: 479.6 ± 46.2 μm; $p = .008$, *t*-test). At 18 weeks, control and KOs were statistically similar (controls: 443.2 ± 30.4 μm; KOs: 426.3 ± 28.8 μm; $p = .769$, t-test). Among control cells, there was a significant increase in inner molecular layer length with age ($p = .009$, t-test). KO cells, on the other hand, did not exhibit growth in the inner molecular layer between 7 and 18 weeks ($p = .423$, t-test). Within the middle molecular layer, PTEN KO cells exhibited greater dendrite length than controls at 7 weeks (Graphs not shown; controls: 891.1 ± 84.5 μm; KOs: 1286.9 ± 106.3; $p = .007$, t-test) but not 18 weeks (controls: 1239.0 ± 60.1 μm; KOs: 1557.9 ± 155.2 μm; $p = .027$, t-test [threshold p value = .0125]). Among control cells – similar to the inner molecular layer – there was an increase in length with age ($p = .001$, *t*-test). Middle molecular layer length did not change with age among KOs ($p = .156$, t-test). Finally, within the outer molecular layer, KO cells exhibited significantly greater length than controls at both time points (Fig. 2D; 7 weeks: $p \leq .001$, *t*-test; 18 weeks, $p \leq .001$, RST). Both controls ($p = .002$, RST) and KOs ($p \leq .001$, RST) exhibited dendritic growth in the outer molecular layer with age. Taken together, these observations are consistent with faster maturation in the inner and middle molecular layers, with KO cells achieving mature lengths more rapidly than controls, but then plateauing once the normal length is reached. In the outer molecular layer, KO cells also appear to grow faster. In this region, however, growth continues in excess of normal values (Fig. 2D).

As an additional measure of dendritic growth, we quantified the number of dendritic branches per molecular layer subregion. Average inner molecular layer branch number was similar between KOs and age-matched controls at 7 (Graphs not shown; controls: 2.7 ± 0.3 branches; KOs: 3.1 ± 0.5; $p = .571$, *t*-test) and 18 weeks (controls: 3 [1–4]; KOs: 5 [3–5]; $p = .036$, RST [threshold p value = .0125]). There was no effect of age among either controls ($p = .769$, t-test) or KO cells ($p = .175$, t-test). In the middle molecular layer, KO cells exhibited significantly more branches than age-matched controls at 7 (Graphs not shown; controls: 1.9 ± 0.3; KOs: 4.3 ± 0.7; $p = .005$, t-test) and 18 weeks (controls: 2[1–3]; KOs: 6[5–9]; $p \leq .001$, RST). Branch number within the middle molecular layer did not change with age for controls ($p = 1.000$, RST) or KOs ($p = .047$, t-test [threshold p value = .0125]). Finally, analysis of dendrite branching in the outer molecular layer revealed a significant difference between KOs and controls, with KOs having greater numbers at both 7 (Fig. 2E, $p \leq .001$, RST) and 18 weeks ($p < .001$; RST). Moreover, while there was no increase with age in outer molecular layer branching for control cells ($p = .052$, RST), branching increased significantly with age among KO cells ($p \leq .0001$, t-test).

These results demonstrate that PTEN deletion alters the character and temporal pattern of granule cell apical dendrite growth. Control cells exhibit modest increases in dendritic length in all three molecular layer subregions with age, but no change in branches. This indicates that growth occurs mainly via extension of existing branches. By contrast, KO cells – which already exhibit larger dendritic trees than controls by 7-weeks-of-age – exhibit the most pronounced growth in the outer molecular layer. This growth is achieved by increased length and branching. Consistent with these quantitative measures, qualitative observation of KO cells dendritic trees revealed unusual extensions of the very distal dendrites of these cells in the outer molecular layer. In control animals, granule cell dendrites extend out to the hippocampal fissure and terminate. However, KO cells dendrites extend out to the fissure and, instead of terminating, turn 90° and continue to grow parallel to the fissure (Fig. 1D, inset). We postulate that these extensions could reflect a failure of normal growth termination signals and protracted expansion of the dendritic tree over time.

3.5. PTEN KO cell abnormalities are more pronounced in animals with greater numbers of KO cells

Having shown that KO cells undergo progressive growth with age, we next queried whether the percentage or load of KO granule cells in the dentate gyrus impacted KO cell structure. There are multiple potential mechanisms by which this might occur, including greater incidence of seizures in higher KO mice (Pun et al., 2012) and localized effects of KO cell clusters. For this experiment, two and three-week-old double-transgenic *Gli1-CreER^{T2}* hemizygous; PTEN$^{flox/flox}$ mice were treated with tamoxifen. In these animals, morphology was revealed by biocytin-filling single cells in acute hippocampal slices. The approach yielded 57 cells from 42 mice, covering an age range of 9–33 weeks.

3.6. Apical dendrite length increases with age and KO cell load

Animals exhibited PTEN deletion rates of 2.0–36.5%, providing a good range for regression analyses. Examples of slices from KO animals are shown in Fig. 3 and individual KO cells from animals with a range of KO cell rates are shown in Fig. 4. Since we previously established that morphology varied with animal age, this was included as a variable in the statistical approach. Animal age was predictive of soma area, but the percentage of KO cells was not predictive (Fig. 5A). Both age and the percentage of KO cells were predictive of total dendritic length (Fig. 5B). The total number of dendritic branches, however, was not predicted from either age or %KO, although clear trends were evident (Fig. 5C).

To further delineate how granule cell structure was changing, dendritic trees were broken down into inner, middle and outer molecular layer subregions. Dendritic length in the inner molecular layer was predicted by the percentage of KO cells, but not by animal age (Fig. 5D). In the middle (Fig. 5E) and outer (Fig. 5F) molecular layers, both age and the percentage of KO cells predicted dendrite length.

Dendritic branching in the inner, middle and outer molecular layers was also examined (graphs not shown). Inner molecular layer branching was not predicted by age ($p = .822$) or the percentage of KO

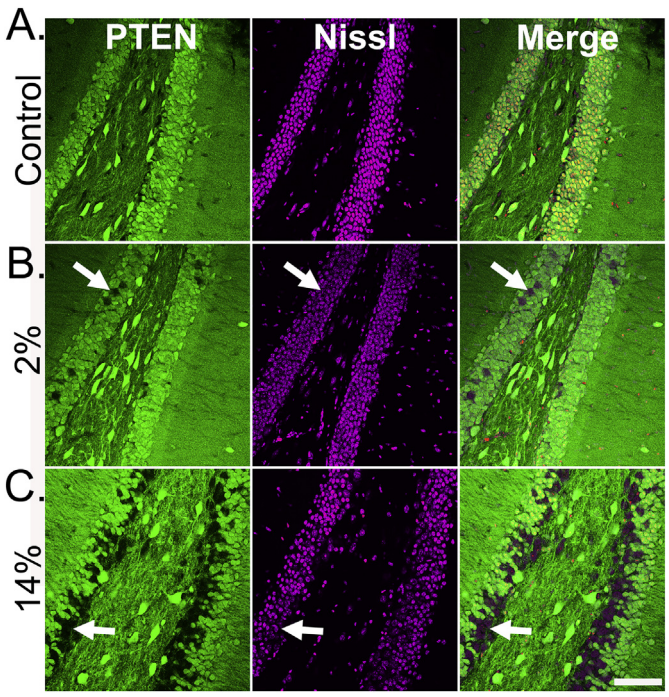

Fig. 3. Titrating the "load" of PTEN KO cells to achieve variable deletion rates. Images are confocal optical sections of the dentate gyrus showing PTEN-expressing cells (green) and Nissl staining (purple) in control mice (row A) and mice with 2% (row B) and 14% (row C) deletion rates. PTEN KO cells appear purple in the merged images (white arrows). Note the concentration of KO cells within the inner third of the dentate granule cell body layer; the typical positioning of postnatally-generated neurons. Scale bar = 50 μm. (For interpretation of the references to colour in this figure legend, the reader is referred to the web version of this article.)

cells (p = .329). Findings were similar for age (p = .230) and the percentage of KO cells (p = .182) in the middle molecular layer. Similar to brainbow-expressing animals, age showed a trend towards being predictive of branch frequency in the outer molecular layer (p = .093). No relationship between outer molecular layer branching and KO cell percentage was found (p = .798).

3.7. Basal dendrite length increases with age among PTEN KO cells

PTEN deletion frequently leads to the formation of basal dendrites projecting into the dentate hilus. While brainbow expression did not reliably reveal basal dendrites in thick sections, basal dendrites were clearly visible among biocytin-filled PTEN KO cells (Fig. 6A). Notably, 75% of KO granule cells had at least one basal dendrite, with a median of one per cell and a range of 0–4. Basal dendrite length was predicted by age but not the percentage of KO cells in the animal, indicating that basal dendrites also grow over time, similar to apical dendrites (Fig. 6B).

3.8. Differences in tamoxifen treatment cannot account for the observed findings among KO cells

To generate the range of KO cell percentiles utilized for the present study, animals were treated with 250 mg/kg tamoxifen on either P14 or P21. With this approach, tamoxifen dose is held constant, but animal age varied. As desired, animals treated on P14 exhibited higher percentages of KO granule cells than animals treated on P21, reflecting the overall decline in neurogenesis rates over this period (P14, n = 42 cells, 25.2% PTEN KO [range = 14.9–36.5]; P21, n = 15 cells, 13.0% [range = 2.0–23.3]; p < .001, t-test). To confirm that the observed effects were not due to this difference in treatment age among animals, regression analyses were repeated using P14 animals only for measures that generated significant outcomes. Results were qualitatively similar. Apical dendrite length was predicted by both age (p = .001; Multiple Linear Regression) and the percentage of KO cells (p = .013) for the P14 group. Inner molecular layer length maintained a strong trend towards being significantly correlated with the percentage of KO cells (p = .057) and middle molecular layer length was predicted by both age (p = .049) and the percentage of KO cells (p = .023). Outer molecular layer length and basal dendrite length were still predicted by age (OML, p < .001; basal dendrites, p = .014). These findings indicate

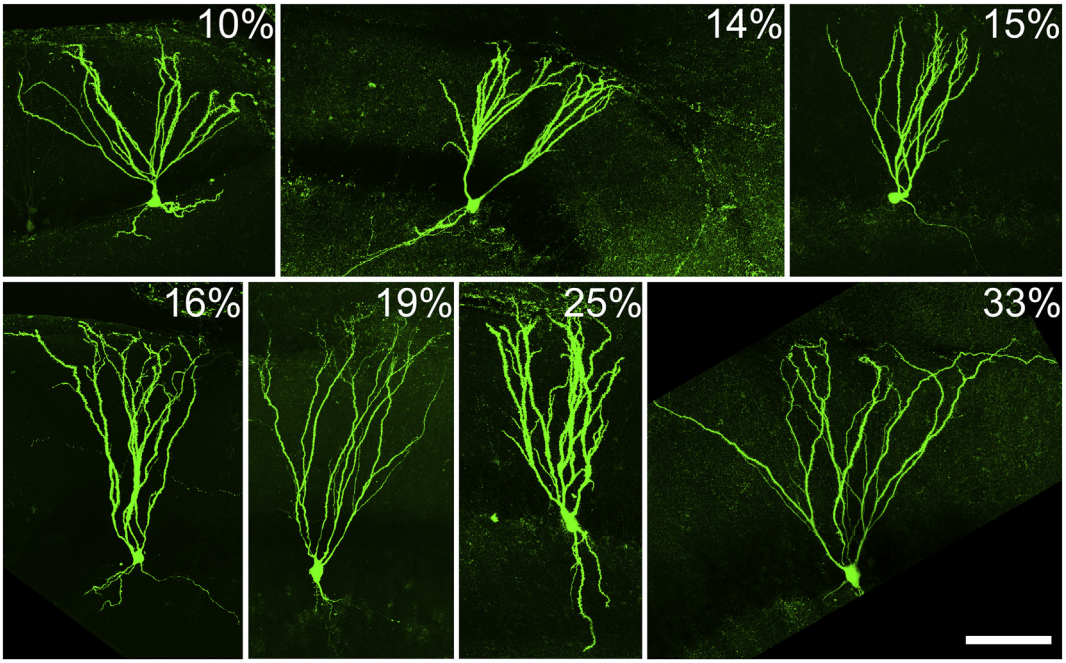

Fig. 4. Neuronal reconstructions of biocytin-filled cells from mice with variable rates of PTEN deletion from the dentate gyrus (10–33%). Cells from animals with higher deletion rates show greater dendritic length and complexity. Scale bar = 100 μm.

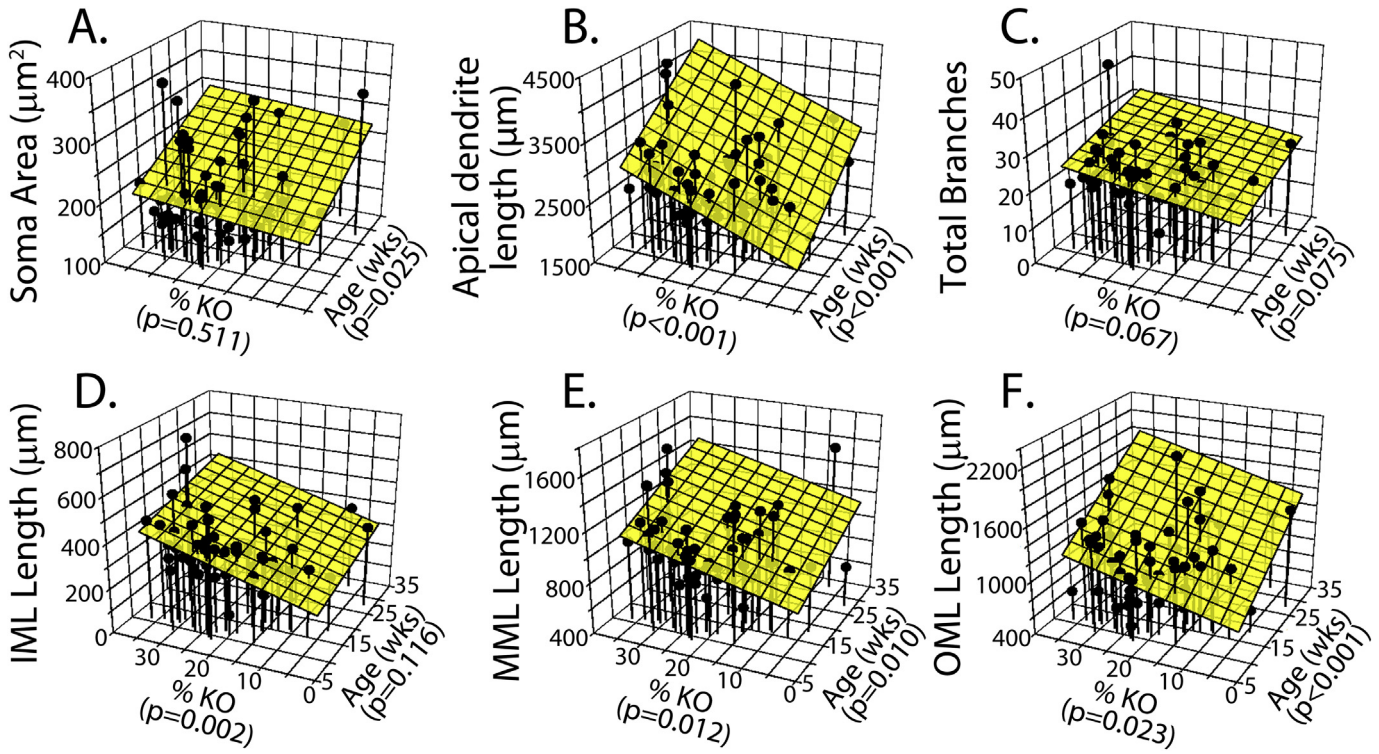

Fig. 5. Three dimensional plots of multiple linear regression analyses utilizing the percentage of KO cells (% KO) and animal age in weeks (wks) as independent variables. The dependent variables are shown on the y-axis for each graph. Soma area (A) was predicted by age only, while apical dendrite length (B) was predicted by both age and the percentage of KO cells. When dendrite length was examined by subregion, dendritic length in the inner molecular layer (IML, D) was predicted by %KO only, while both variables predicted length in the middle (MML, E) and outer (OML, F) molecular layers. *P*-values for each independent variable are given on the appropriate axis.

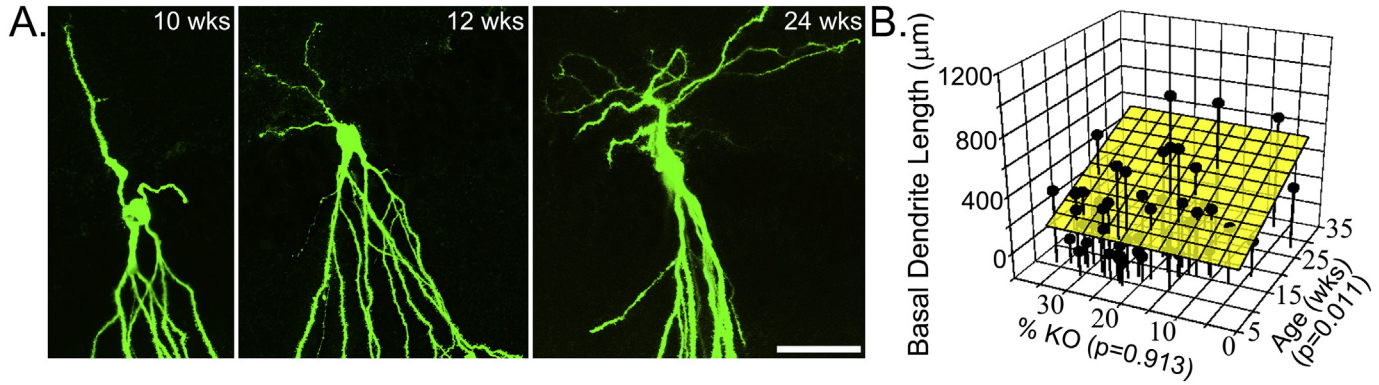

Fig. 6. Basal dendrite length is predicted by animal age. A: Images show neuronal reconstructions of PTEN KO granule cells from mice at 10–24 weeks (wks)-of-age. Basal dendrites are shown projecting upwards. Scale bar = 50 μm. B: The three-dimensional plot depicts the results of a multiple linear regression analysis with the percentage of KO cells (%KO) and animal age (wks) as independent variables and basal dendrite length as the dependent variable. Basal dendrite length was predicted by animal age. *P* values are provided on the appropriate axis.

that the observed increases in dendritic length with age and KO cell load are not artifacts of the tamoxifen dosing paradigm.

4. Discussion

Mutations that increase mTOR pathway signaling cause numerous human diseases. Because mutations can be germline or somatic in nature, the number of affected cells can vary widely across patients. Here, we utilized a granule cell-specific PTEN knockout (KO) mouse model to determine whether variations in the number of affected cells impacts the morphological development of these same cells, or whether aberrant cell growth occurs independently of affected cell number. The latter would suggest aberrant growth is driven entirely by PTEN loss in the affected cell, while the former implies that paracrine and/or secondary effects contribute (Fig.7). We also examined the impact of animal age on KO cell morphology, as secondary pathologies, such as inflammation and seizures, become more severe with time. Both animal age and the load of PTEN KO cells were significant predictors of KO cell morphology over an age range of 8 months. These findings indicate that PTEN deletion leads to a chronic and progressive dysmorphogenesis of granule cell structure, with abnormalities increasing in severity as a function of age and KO cell number. The mechanism(s) underlying these phenomena remain to be elucidated, however, the findings imply that pathological changes among individual mutant cells may be greater in patients with greater numbers of mutant cells.

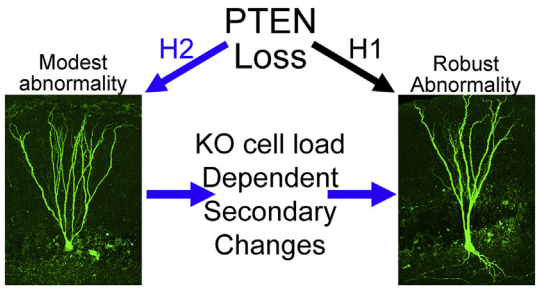

Fig. 7. The present study tested two competing hypotheses. The simplest hypothesis (H1, black arrow) predicts that KO granule cell morphology is entirely driven by cell intrinsic effects of PTEN loss. The key prediction of this model is that there should be no relationship between the number of KO cells in an animal and the morphology of individual KO cells. Our data supports the alternate hypothesis (H2, blue arrows), which predicts that the cell intrinsic effects of PTEN loss act in concert with secondary changes induced by the abnormal cells to exacerbate aberrant morphological changes among KO cells. (For interpretation of the references to colour in this figure legend, the reader is referred to the web version of this article.)

4.1. Potential mechanisms of PTEN KO cell "load" effects

Abundant evidence from animal models and human mTORopathies supports the conclusion that the load of mutant cells affects disease severity at the whole organism level. In our original paper describing the PTEN model, we found that animals with PTEN loss from > 10% of the granule cell population developed cortical seizures, while animals with lower deletion rates did not develop cortical seizures (Pun et al., 2012). Similarly, deletion of PTEN using promoters that target most neurons (NSE-cre; GFAP-cre) produce gross brain abnormalities that are absent from our granule cell specific model (Kwon et al., 2001, 2006; Fraser et al., 2004; Ljungberg et al., 2009). Clinically, patients with restricted mosaicism have milder disease than patients with constitutional mutations (Alcantara et al., 2017). The novel finding here is the observation that *individual* PTEN KO cells develop larger dendritic trees in animals with greater overall numbers of KO cells.

A number of possibilities can be considered to explain the observed relationship between KO cell load and KO cell size. Firstly, we note that the experimental design precludes the possibility that experimenter bias could account for the observed relationship. In this model, KO cell load cannot be established until immunohistochemical experiments are completed on collected brain slices – weeks after biocytin fills are done. In addition, optical imaging of slices was only used to place the patch pipette above the inner third of granule cell body layer. Individual somas were not visualized or targeted to avoid bias towards larger cells. We note, however, that correlative data can sometimes be misleading, so the possibility of an artifactual finding cannot be entirely dismissed. We cannot exclude the possibility, for example, that technical factors might favor successful patching of larger cells in animals with higher KO rates – although we are unaware of any mechanism the might produce such a bias. Of greater interest, plausible biological mechanisms could also produce the observed relationship. Animals with higher percentages of PTEN KO granule cells exhibit hypertrophy of the dentate gyrus, modest increases in reactive gliosis, abnormal hippocampal physiology, seizures and premature mortality (Pun et al., 2012; LaSarge et al., 2016; Santos et al., 2017). These changes, alone or in combination, could act to stimulate granule cell growth (Fig. 7). Hypertrophy of the dentate gyrus – induced by large numbers of KO cells developing somas and dendrites 3–4 times larger and thicker than controls – might induce further expansion of the dendritic tree by creating more space to grow. Alternatively, seizures could serve as a stimulus for neuronal growth. mTOR pathway activation is highly responsive to neuronal activity (Takei and Nawa, 2014) and acts to promote activity-dependent neuronal growth and plasticity (Von Der Brelie et al., 2006; Hoeffer and Klann, 2010). The onset of seizures in higher KO animals might create a positive feedback loop, whereby KO cells become increasingly abnormal in response to heightened activity levels. If either of these latter possibilities is confirmed, it may be possible to reduce mTOR-mediated neuronal dysmorphogenesis by controlling secondary changes.

4.2. PTEN deletion alters neuronal growth patterns

In the first set of experiments presented here (Fig. 2), control and PTEN KO cells were examined in 7- and 18-week-old mice. Because fluorophore-expression was induced among progenitor cells when the animals were 3 weeks old, the ages of the cells examined would be 4 and 15 weeks, respectively. By 4–6 weeks of age, granule cells are functionally mature, with dendrites reaching the hippocampal fissure, axons in the hilus and CA3 stratum lucidum, and the ability to fire action potential and activate downstream targets (Overstreet-Wadiche and Westbrook, 2006; Zhao et al., 2006; Ge et al., 2007; Toni et al., 2008; Gu et al., 2012). Studies of adult neurogenesis, however, indicate that additional physiological and morphological changes occur beyond the period of initial functional maturity (van Praag et al., 2002; Zhao et al., 2006). The present results are in accord with these findings, with control granule cells exhibiting dendritic lengthening between the two time points. KO granule cell dendrites also increased in length, but achieved significantly larger trees than controls via a combination of dendritic lengthening and increased branching. Moreover, the second set of experiments presented here revealed that KO cell dendritic trees continue to increase in size for up to 8 months (Fig. 5).

The relative contributions of KO cell load and age to granule cell dysmorphogenesis cannot be fully discriminated here. PTEN loss may directly promote prolonged neuronal growth at the level of individual neurons, accounting for the observed association between dendritic size and age. Disease severity in the PTEN model, however, also becomes more severe with age (Pun et al., 2012), and could underlie the positive correlation between age and dendritic extent. We did include an age*% KO interaction term in our analyses, but no significant interactions were found (data not shown). Examination of animals with very low loads of KO cells (< 1%) in future studies, in which the disease phenotype is absent, will be needed to fully resolved the relationship between age and KO cell load.

4.3. Functional impact of morphological changes

A modest increase in basal dendrite length with age was noted among KO cells. Basal dendrites are rare among control cells, and these aberrant processes provide a pathway for recurrent circuit formation within the dentate (Ribak et al., 2000; Kelly and Beck, 2017). Indeed, physiological evidence of recurrent activity is observed in this model following perforant pathway activation in acute hippocampal slices (Lasarge et al., 2016). Slices from control animals exhibit only a single population spike following stimulation, while slices from KO animals consistently exhibit multiple spikes – indicative of recurrent circuitry. Continued basal dendrite growth suggests this recurrent pathway may become more robust over time. Growth of apical dendrites may also contribute to hyperexcitability in these animals by providing a substrate for increased input from entorhinal cortex, a finding consistent with evidence of increased spontaneous excitatory postsynaptic currents among KO granule cells (Santos et al., 2017).

4.4. Time window for intervention in mTORopathies

The protracted time period over which PTEN deletion promotes neuronal dysmorphogenesis has implications for mTORopathies. Specifically, while some PTEN-induced neuronal changes can be reversed by treatment with the mTOR antagonist rapamycin, others cannot. Somatic hypertrophy, for example, can be prevented and

reversed with rapamycin (Getz et al., 2016). Aberrant neuronal migration, on the other hand, was not reversible (Williams et al., 2016). Whether or not the progressive increases in apical and basal dendrite length observed here can be reversed remains to be determined, but the present findings indicate that the window for preventative treatment is large. These observations are consistent with studies showing that delayed rapamycin treatment is still effective in PTEN KO models of epilepsy (Sunnen et al., 2011; Nguyen et al., 2015). Similarly, this could contribute to the efficacy of rapalogues (such as the mTOR antagonist everolimus) to produce positive effects in clinical trials in patients with tuberous sclerosis complex and refractory partial onset seizures (Krueger et al., 2013, 2016) (EXIST-3, ClinicalTrials.gov identifier: NCT01713946). Results from the present study indicate that both early and late treatment with mTOR antagonists may prevent neuronal dysmorphogenesis.

5. Conclusions

mTOR pathway mutations are linked to autism spectrum disorder, brain malformations and epilepsy (Conti et al., 2012; Marchese et al., 2014). Mosaicism in these patients can produce widely varying numbers of mutant cells. Our findings indicate that the dendritic growth of individual KO cells is greater in animals with greater numbers of KO cells, implying that disease severity in patients may reflect the combinatorial effects of the total size of the mutant cell population, and the severity of abnormalities exhibited by individual mutant cells. We also find that PTEN loss produces chronic changes in neuronal growth. Encouragingly, these observations imply that the potential treatment window for preventing neuronal dysmorphogenesis is large, extending well-beyond the phase of neuronal differentiation.

Acknowledgments

We would like to thank Keri Kaeding for useful comments on this manuscript and Dr. Lili Ding (CCHMC) for help with statistical analyses. We also would like to thank the Cincinnati Children's Hospital Medical Center Confocal Imaging Core for their assistance with confocal image acquisition and analysis.

Funding

This work was supported by the National Institute of Neurological Disorders and Stroke (SCD, Awards R01NS065020 and R01NS062806; CLL, F32NS083239).

Conflict of interest

The authors have nothing to report.

References

Ahn, S., Joyner, A.L., 2005. In vivo analysis of quiescent adult neural stem cells responding to Sonic hedgehog. Nature 437 (7060), 894.

Alcantara, D., Timms, A.E., Gripp, K., Baker, L., Park, K., Collins, S., Cheng, C., Stewart, F., Mehta, S.G., Saggar, A., Sztriha, L., Zombor, M., Caluseriu, O., Mesterman, R., Van Allen, M.I., Jacquinet, A., Ygberg, S., Bernstein, J.A., Wenger, A.M., Guturu, H., Bejerano, G., Gomez-Ospina, N., Lehman, A., Alfei, E., Pantaleoni, C., Conti, V., Guerrini, R., Moog, U., Graham Jr., J.M., Hevner, R., Dobyns, W.B., O'Driscoll, M., Mirzaa, G.M., 2017. Mutations of AKT3 are associated with a wide spectrum of developmental disorders including extreme megalencephaly. Brain 140 (10), 2610–2622.

Amaral, D.G., Scharfman, H.E., Lavenex, P., 2007. The dentate gyrus: fundamental neuroanatomical organization (dentate gyrus for dummies). Prog. Brain Res. 163, 3–790.

Amiri, A., Cho, W., Zhou, J., Birnbaum, S.G., Sinton, C.M., McKay, R.M., Parada, L.F., 2012. Pten deletion in adult hippocampal neural stem/progenitor cells causes cellular abnormalities and alters neurogenesis. J. Neurosci. 32 (17), 5880–5890.

Backman, S.A., Stambolic, V., Suzuki, A., Haight, J., Elia, A., Pretorius, J., Tsao, M.-S., Shannon, P., Bolon, B., Ivy, G.O., 2001. Deletion of Pten in mouse brain causes seizures, ataxia and defects in soma size resembling Lhermitte-Duclos disease. Nat. Genet. 29 (4), 396–404.

Barrows, C.M., McCabe, M.P., Chen, H., Swann, J.W., Weston, M.C., 2017. PTEN loss increases the Connectivity of Fast Synaptic Motifs and Functional Connectivity in a developing Hippocampal Network. J. Neurosci. 37 (36), 8595–8611.

Cai, D., Cohen, K.B., Luo, T., Lichtman, J.W., Sanes, J.R., 2013. Improved tools for the Brainbow toolbox. Nat. Methods 10 (6), 540–547.

Conti, S., Condo, M., Posar, A., Mari, F., Resta, N., Renieri, A., Neri, I., Patrizi, A., Parmeggiani, A., 2012. Phosphatase and tensin homolog (PTEN) gene mutations and autism: literature review and a case report of a patient with Cowden syndrome, autistic disorder, and epilepsy. J. Child Neurol. 27 (3), 392–397.

Crino, P.B., 2011. mTOR: a pathogenic signaling pathway in developmental brain malformations. Trends Mol. Med. 17 (12), 734–742.

Deller, T., Drakew, A., Frotscher, M., 1999. Different primary target cells are important for fiber lamination in the fascia dentata: a lesson from reeler mutant mice. Exp. Neurol. 156 (2), 239–253.

Dimoka, A., Courellis, S., Song, D., Marmarelis, V., Bergpr, T., 2003. Identification of the lateral and medial perforant path of the hippocampus using single and dual random impulse train stimulation. Engineering in Medicine and Biology Society, 2003. In: Proceedings of the 25th Annual International Conference of the IEEE. IEEE.

Förster, E., Zhao, S., Frotscher, M., 2006. Laminating the hippocampus. Nat. Rev. Neurosci. 7 (4), 259–268.

Fraser, M.M., Zhu, X., Kwon, C.H., Uhlmann, E.J., Gutmann, D.H., Baker, S.J., 2004. Pten loss causes hypertrophy and increased proliferation of astrocytes in vivo. Cancer Res. 64 (21), 7773–7779.

Ge, S., Yang, C.-h., Hsu, K.-s., Ming, G.-l., Song, H., 2007. A critical period for enhanced synaptic plasticity in newly generated neurons of the adult brain. Neuron 54 (4), 559–566.

Getz, S.A., Despenza, T., Li, M., Luikart, B.W., 2016. Rapamycin prevents, but does not reverse, aberrant migration in Pten knockout neurons. Neurobiol. Dis. 93, 12–20.

Gu, Y., Arruda-Carvalho, M., Wang, J., Janoschka, S.R., Josselyn, S.A., Frankland, P.W., Ge, S., 2012. Optical controlling reveals time-dependent roles for adult-born dentate granule cells. Nat. Neurosci. 15 (12), 1700–1706.

Hama, H., Hioki, H., Namiki, K., Hoshida, T., Kurokawa, H., Ishidate, F., Kaneko, T., Akagi, T., Saito, T., Saido, T., Miyawaki, A., 2015. ScaleS: an optical clearing palette for biological imaging. Nat. Neurosci. 18 (10), 1518–1529.

Hoeffer, C.A., Klann, E., 2010. mTOR signaling: at the crossroads of plasticity, memory and disease. Trends Neurosci. 33 (2), 67–75.

Jaworski, J., Spangler, S., Seeburg, D.P., Hoogenraad, C.C., Sheng, M., 2005. Control of dendritic arborization by the phosphoinositide-3′-kinase–Akt–mammalian target of rapamycin pathway. J. Neurosci. 25 (49), 11300–11312.

Kelly, T., Beck, H., 2017. Functional properties of granule cells with hilar basal dendrites in the epileptic dentate gyrus. Epilepsia 58 (1), 160–171.

Krueger, D.A., Wilfong, A.A., Holland-Bouley, K., Anderson, A.E., Agricola, K., Tudor, C., Mays, M., Lopez, C.M., Kim, M.O., Franz, D.N., 2013. Everolimus treatment of refractory epilepsy in tuberous sclerosis complex. Ann. Neurol. 74 (5), 679–687.

Krueger, D.A., Wilfong, A.A., Mays, M., Talley, C.M., Tudor, C., Capal, J., Holland-Bouley, K., Franz, D.N., 2016. Long-term treatment of epilepsy with everolimus in tuberous sclerosis. Neurology 87 (23), 2408–2415.

Kwon, C.-H., Zhu, X., Zhang, J., Knoop, L.L., Tharp, R., Smeyne, R.J., Eberhart, C.G., Burger, P.C., Baker, S.J., 2001. Pten regulates neuronal soma size: a mouse model of Lhermitte-Duclos disease. Nat. Genet. 29 (4), 404–411.

Kwon, C.-H., Zhu, X., Zhang, J., Baker, S.J., 2003. mTor is required for hypertrophy of Pten-deficient neuronal soma in vivo. Proc. Natl. Acad. Sci. 100 (22), 12923–12928.

Kwon, C.-H., Luikart, B.W., Powell, C.M., Zhou, J., Matheny, S.A., Zhang, W., Li, Y., Baker, S.J., Parada, L.F., 2006. Pten regulates neuronal arborization and social interaction in mice. Neuron 50 (3), 377–388.

Lasarge, C.L., Danzer, S.C., 2014. Mechanisms regulating neuronal excitability and seizure development following mTOR pathway hyperactivation. Front. Mol. Neurosci. 7.

Lasarge, C.L., Santos, V.R., Danzer, S.C., 2015. PTEN deletion from adult-generated dentate granule cells disrupts granule cell mossy fiber axon structure. Neurobiol. Dis. 75, 142–150.

Lasarge, C.L., Pun, R.Y., Muntifering, M.B., Danzer, S.C., 2016. Disrupted hippocampal network physiology following PTEN deletion from newborn dentate granule cells. Neurobiol. Dis. 96, 105–114.

Ljungberg, M.C., Sunnen, C.N., Lugo, J.N., Anderson, A.E., D'Arcangelo, G., 2009. Rapamycin suppresses seizures and neuronal hypertrophy in a mouse model of cortical dysplasia. Dis. Model. Mech. 2 (7–8), 389–398.

Lugo, J.N., Smith, G.D., Arbuckle, E.P., White, J., Holley, A.J., Floruta, C.M., Ahmed, N., Gomez, M.C., Okonkwo, O., 2014. Deletion of PTEN produces autism-like behavioral deficits and alterations in synaptic proteins. Front. Mol. Neurosci. 7, 27.

Luikart, B.W., Schnell, E., Washburn, E.K., Bensen, A.L., Tovar, K.R., Westbrook, G.L., 2011. Pten knockdown in vivo increases excitatory drive onto dentate granule cells. J. Neurosci. 31 (11), 4345–4354.

Marchese, M., Conti, V., Valvo, G., Moro, F., Muratori, F., Tancredi, R., Santorelli, F.M., Guerrini, R., Sicca, F., 2014. Autism-epilepsy phenotype with macrocephaly suggests PTEN, but not GLIALCAM, genetic screening. BMC Med Genet 15, 26.

Marsan, E., Baulac, S., 2018 Feb. (2018). Review: Mechanistic target of rapamycin (mTOR) pathway, focal cortical dysplasia and epilepsy. Neuropathol. Appl. Neurobiol. 44 (1), 6–17.

Matsushita, Y., Sakai, Y., Shimmura, M., Shigeto, H., Nishio, M., Akamine, S., Sanefuji, M., Ishizaki, Y., Torisu, H., Nakabeppu, Y., 2016. Hyperactive mTOR signals in the proopiomelanocortin-expressing hippocampal neurons cause age-dependent epilepsy and premature death in mice. Sci. Rep. 6, 22991.

Murphy, B.L., Pun, R.Y., Yin, H., Faulkner, C.R., Loepke, A.W., Danzer, S.C., 2011. Heterogeneous integration of adult-generated granule cells into the epileptic brain. J. Neurosci. 31 (1), 105–117.

Nguyen, L.H., Anderson, A.E., 2018. mTOR-dependent alterations of Kv1.1 subunit

expression in the neuronal subset-specific Pten knockout mouse model of cortical dysplasia with epilepsy. Sci. Rep. 8 (1), 3568.
Nguyen, L.H., Brewster, A.L., Clark, M.E., Regnier-Golanov, A., Sunnen, C.N., Patil, V.V., D'Arcangelo, G., Anderson, A.E., 2015. mTOR inhibition suppresses established epilepsy in a mouse model of cortical dysplasia. Epilepsia 56 (4), 636–646.
Ogawa, S., Kwon, C.-H., Zhou, J., Koovakkattu, D., Parada, L.F., Sinton, C.M., 2007. A seizure-prone phenotype is associated with altered free-running rhythm in Pten mutant mice. Brain Res. 1168, 112–123.
Overstreet-Wadiche, L.S., Westbrook, G.L., 2006. Functional maturation of adult-generated granule cells. Hippocampus 16 (3), 208–215.
Parker, W.E., Orlova, K.A., Parker, W.H., Birnbaum, J.F., Krymskaya, V.P., Goncharov, D.A., Baybis, M., Helfferich, J., Okochi, K., Strauss, K.A., 2013. Rapamycin prevents seizures after depletion of STRADA in a rare neurodevelopmental disorder. Sci. Transl. Med. 5 (182), 182ra153.
Paxinos, G., Franklin, K.B.J., 2004. The Mouse Brain in Stereotaxic Coordinates, 2nd Edition. Academic Press.
Pinault, D., 1996. A novel single-cell staining procedure performed in vivo under electrophysiological control: morpho-functional features of juxtacellularly labeled thalamic cells and other central neurons with biocytin or Neurobiotin. J. Neurosci. Methods 65 (2), 113–136.
Pun, R.Y., Rolle, I.J., Lasarge, C.L., Hosford, B.E., Rosen, J.M., Uhl, J.D., Schmeltzer, S.N., Faulkner, C., Bronson, S.L., Murphy, B.L., 2012. Excessive activation of mTOR in postnatally generated granule cells is sufficient to cause epilepsy. Neuron 75 (6), 1022–1034.
Ribak, C.E., Tran, P.H., Spigelman, I., Okazaki, M.M., Nadler, J.V., 2000. Status epilepticus-induced hilar basal dendrites on rodent granule cells contribute to recurrent excitatory circuitry. J. Comp. Neurol. 428 (2), 240–253.
Santos, V.R., de Castro, O.W., Pun, R.Y., Hester, M.S., Murphy, B.L., Loepke, A.W., Garcia-Cairasco, N., Danzer, S.C., 2011. Contributions of mature granule cells to structural plasticity in temporal lobe epilepsy. Neuroscience 197, 348–357.
Santos, V.R., Pun, R.Y., Arafa, S.R., Lasarge, C.L., Rowley, S., Khademi, S., Bouley, T., Holland, K.D., Garcia-Cairasco, N., Danzer, S.C., 2017. PTEN deletion increases hippocampal granule cell excitability in male and female mice. Neurobiol. Dis. 108, 339–351.
Singh, S.P., Lasarge, C.L., An, A., McAuliffe, J.J., Danzer, S.C., 2015. Clonal Analysis of Newborn Hippocampal Dentate Granule Cell Proliferation and Development in Temporal Lobe Epilepsy. eNeuro 2 (6).
Sperow, M., Berry, R.B., Bayazitov, I.T., Zhu, G., Baker, S.J., Zakharenko, S.S., 2012. Phosphatase and tensin homologue (PTEN) regulates synaptic plasticity independently of its effect on neuronal morphology and migration. J. Physiol. 590 (4), 777–792.
Sunnen, C.N., Brewster, A.L., Lugo, J.N., Vanegas, F., Turcios, E., Mukhi, S., Parghi, D., D'Arcangelo, G., Anderson, A.E., 2011. Inhibition of the mammalian target of rapamycin blocks epilepsy progression in NS-Pten conditional knockout mice. Epilepsia 52 (11), 2065–2075.
Takei, N., Nawa, H., 2014. mTOR signaling and its roles in normal and abnormal brain development. Front. Mol. Neurosci. 7.
Toni, N., Laplagne, D.A., Zhao, C., Lombardi, G., Ribak, C.E., Gage, F.H., Schinder, A.F., 2008. Neurons born in the adult dentate gyrus form functional synapses with target cells. Nat. Neurosci. 11 (8), 901–907.
Urbanska, M., Gozdz, A., Swiech, L.J., Jaworski, J., 2012. Mammalian target of rapamycin complex 1 (mTORC1) and 2 (mTORC2) control the dendritic arbor morphology of hippocampal neurons. J. Biol. Chem. 287 (36), 30240–30256.
van Groen, T., Miettinen, P., Kadish, I., 2003. The entorhinal cortex of the mouse: organization of the projection to the hippocampal formation. Hippocampus 13 (1), 133–149.
van Praag, H., Schinder, A.F., Christie, B.R., Toni, N., Palmer, T.D., Gage, F.H., 2002. Functional neurogenesis in the adult hippocampus. Nature 415 (6875), 1030–1034.
Von Der Brelie, C., Waltereit, R., Zhang, L., Beck, H., Kirschstein, T., 2006. Impaired synaptic plasticity in a rat model of tuberous sclerosis. Eur. J. Neurosci. 23 (3), 686–692.
Walter, C., Murphy, B.L., Pun, R.Y., Spieles-Engemann, A.L., Danzer, S.C., 2007. Pilocarpine-induced seizures cause selective time-dependent changes to adult-generated hippocampal dentate granule cells. J. Neurosci. 27 (28), 7541–7552.
Wesseling, H., Elgersma, Y., Bahn, S., 2017. A brain proteomic investigation of rapamycin effects in the Tsc1 +/− mouse model. Mol Autism 8, 41.
West, M.J., Andersen, A.H., 1980. An allometric study of the area dentata in the rat and mouse. Brain Res. Rev. 2 (1), 317–348.
Williams, M.R., Despenza, T., Li, M., Gulledge, A.T., Luikart, B.W., 2015. Hyperactivity of newborn Pten knock-out neurons results from increased excitatory synaptic drive. J. Neurosci. 35 (3), 943–959.
Williams, M.R., Fricano-Kugler, C.J., Getz, S.A., Skelton, P.D., Lee, J., Rizzuto, C.P., Geller, J.S., Li, M., Luikart, B.W., 2016. A retroviral CRISPR-Cas9 system for cellular autism-associated phenotype discovery in developing neurons. Sci. Rep. 6, 25611.
Wong, M., Crino, P.B., 2012. mTOR and epileptogenesis in developmental brain malformations. In: Noebels, J.L., Avoli, M., Rogawski, M.A., Olsen, R.W., Delgado-Escueta, A.V. (Eds.), Jasper's Basic Mechanisms of the Epilepsies [Internet]. 4th edition National Center for Biotechnology Information (US), Bethesda (MD).
Zeng, L.H., Xu, L., Gutmann, D.H., Wong, M., 2008. Rapamycin prevents epilepsy in a mouse model of tuberous sclerosis complex. Ann. Neurol. 63 (4), 444–453.
Zhao, C., Teng, E.M., Summers Jr., R.G., Ming, G.L., Gage, F.H., 2006. Distinct morphological stages of dentate granule neuron maturation in the adult mouse hippocampus. J. Neurosci. 26 (1), 3–11.
Zhou, J., Blundell, J., Ogawa, S., Kwon, C.-H., Zhang, W., Sinton, C., Powell, C.M., Parada, L.F., 2009. Pharmacological inhibition of mTORC1 suppresses anatomical, cellular, and behavioral abnormalities in neural-specific Pten knock-out mice. J. Neurosci. 29 (6), 1773–1783.